Available online at www.sciencedirect.com
SCIENCE DIRECT
ELSEVIER
Journal of the European Ceramic Society 26 (2006) 1535–1545
ECERS
www.elsevier.com/locate/jeurceramsoc

One-step preparation of size-defined aggregates of TiO_2 nanocrystals with tuning of their phase and composition

Qinghong Zhang, Lian Gao *

State Key Laboratory of High Performance Ceramics and Superfine Microstructure, Shanghai Institute of Ceramics, Chinese Academy of Sciences, 1295 Ding Xi Road, Shanghai 200050, PR China

Received 2 December 2004; received in revised form 25 February 2005; accepted 12 March 2005
Available online 24 May 2005

Abstract

One-step route based on the thermal decomposition of the double salt $(NH_4)_2TiO(SO_4)_2$ (ammonium titanyl sulfate, ATS) is presented to prepare size-defined aggregates of Ti-based nanoparticles with structural hierarchy. The component of Ti-based networks is tunable from anatase/rutile TiO_2, nitrogen-doped TiO_2, TiN_xO_{1-x}, to TiN depending on the atmospheres and reaction temperatures. The as-prepared Ti-based powders were characterized by X-ray diffraction analysis (XRD), transmission electron microscopy (TEM), UV–vis diffuse reflectance spectra (DRS), and BET surface area techniques. It is found that TiO_2 in the predominant rutile phase could be achieved by the thermal decomposition of ATS in flowing Ar gas. Furthermore, the nitrogen-doped TiO_2, TiN_xO_{1-x} solid solution and TiN were prepared by the thermal decomposition of ATS in flowing NH_3 gas by varying the temperatures. The network of anatase TiO_2 with a specific surface area up to 64 $m^2\ g^{-1}$ contains large mesopores with a mean diameter of ca. 15 nm, and the large pore size allows more accessible surface and interface available for the photocatalytic degradation of large-molecule dyes. The photocatalytic activity of the prepared TiO_2 and nitrogen-doped TiO_2 under UV–vis light irradiation is compared to Degussa P-25 using the photocatalytic degradation of methylene blue (MB) as a model reaction. The anatase TiO_2 nanoparticles derived from one-step route show the highly efficient photocatalytic activity for the degradation of MB in comparison with Degussa P-25. The presence of large-sized rutile in the TiO_2 powder decreases the specific surface area and thus the powder exhibits a lower photocatalytic activity.

Keywords: Powders-chemical preparation; Optical properties; TiO_2; Nitrides; Functional applications

1. Introduction

Nanocrystalline TiO_2 powders possess excellent optical, dielectric, and catalytic properties resulting in industrial applications as pigments, solar cells, fillers, opacifiers, and photocatalysts.[1–3] The photocatalytic properties of TiO_2 powders are primarily dependent on particle size, composition, structure and synthetic process.[4–7] The solution-phase chemistry is extensively used to make amorphous or nanocrystalline titania, employs hydrolysis of metal alkoxides or halides.[4,8–10] Wet-chemical routes have multi-fold advantages from the successful preparation of quantum-sized dots to the variable morphology of the resulting nanocrystals. However, nanocrystals obtained from wet chemistry route have fully hydroxylated surfaces unless extreme heat treatments or chemical dehydroxylation reactions are applied. Another problem accompanying the wet-chemical route is that the tedious and repeated washing or leaching of the resulting oxide nanoparticles are absolutely necessary, which results in the difficulty for recovering of organic compounds from liquid medium and makes this process expensive to implement on a large scale. Recently, thermal decomposition of ammonium aluminum carbonate hydroxide and zinc peroxide was used to prepare nanocrystalline α-Al_2O_3[11] and ZnO,[12] respectively. Salt-assisted aerosol decomposition was applied to prepare other oxides with high specific surface area (washing is also needed to remove the salt in the product).[13]

* Corresponding author. Tel.: +86 215 241 2718; fax: +86 215 241 3122.
E-mail address: liangaoc@online.sh.cn (L. Gao).

0955-2219/$ – see front matter © 2005 Elsevier Ltd. All rights reserved.
doi:10.1016/j.jeurceramsoc.2005.03.243

Solution-based non-hydrolytic methods have been developed for successful synthesis of nanocrystalline TiO_2 in the presence of organic compounds as solvent or surfactants.[14] Unfortunately, the organic compounds remnant on the surface of TiO_2 nanoparticles may be undesired for many applications. Moreover, the utilization of organic titanium compounds as precursors or organic microemulsion media encounters the problem of high cost and environmental damage. Recently, Deloume et al. presented the synthesis of TiO_2 photocatalysts based on the molten salts,[15] and repeatedly washing by water was necessary to eliminate the remnant impurities (metal ions Li^+, Na^+ and K^+) on the surface of TiO_2. The notorious NO_2 gas was released during the thermal decomposition of these alkali nitrates, and the obtained TiO_2 powders possess a lower photocatalytic activity compared with Degussa P-25 for the photocatalytic degradation of Prosulfuron®.[15]

The semiconductor–liquid interfaces play an important role in the photocatalytic process,[16] and therefore the porosity and the pore size distribution influence the photocatalytic activity. The beneficial effect of textural meso- and macro-pores on catalysis has been reported by Pinnavaia et al.,[17] and a similar effect for photocatalytic degradation of *n*-pentane in air has been reported for the first time by Zhang and Yu.[18] Mesoporous titania currently exists in two forms, ordered mesoporous titania and nanocrystalline titania.[19] Nanocrystalline titania powders consist of a random agglomeration of titania nanocrystals, and a disordered porous system in the mesopore-size region is created through this type of agglomeration.[19] Many works based on the surfactant-templated approach have been presented to prepare orderedly mesoporous TiO_2 and current efforts focus on improving the crystallization and immobilization of mesoporous TiO_2.[20] The amorphous nature and poor-crystallinity of TiO_2 walls prevent them from being used as highly efficient photocatalyst due to the high hole–electron recombination rate in amorphous TiO_2.[21] The TiO_2 nanoparticles derived from the wet-chemical route generally have a microporous to mesoporous (<10 nm) structure depending on the preparation conditions.[8,22] Extending the range of available pore size and internal surface area is of great interest in catalytic supports, sorbents, and thermal insulation.[23] Three-dimensionally mesoporous architectures with continuous but aperiodically porous networks that wrap around the catalytic solid network offer transport route around blockages.[23] Porosity is an important part of any nanostructured system that does chemistry especially the final chemistry is labeled as heterogeneous catalysis because the reactions are most effective when the transport paths through which molecules move into or out of the nanostructured material are included as an integral part of the architectural design. At present, most templating procedures require one-time-only use of templating materials and auxiliary solvent extraction, which makes such processes industrially uneconomical.[13] To prepare mesoporous TiO_2 with higher photocatalytic activity and from an environmental-benign process is still a challenge.

Thermal decomposition of $Ti(OPr)_4$–stearic acid complex has been presented to prepare TiO_2 nanocrystals with mesopores of 15 nm size.[24] A polymer gel has been used to form porous titania and titania/zirconia,[25] and the resulting porous titania exhibits an efficiency of 60–65% of the standard Degussa P-25 for the photocatalytic degradation of salicylic acid and 2-chlorophenol.[25] Also inorganic salt has been employed as a templating medium to support the developing pore structure with a thermal decomposition process, which allows for a very short time to form a mesoporous nanoarchitecture.[13]

We previously reported the preparation of anatase TiO_2 by the thermal decomposition of AST, and the obtained anatase TiO_2 possesses higher photocatalytic activity than that of Degussa P-25 for the photocatalytic degradation of phenol.[26] In this paper, we extend the thermolysis of AST to prepare Ti-based nanocrystals from anatase TiO_2 to cubic TiN with structural hierarchy. The liberated gas during the thermal decomposition of ATS could be easily recyclable and therefore this process is an environmentally benign route for the preparation of Ti-based powders. Altering the atmosphere for the thermal decomposition of ATS can vary both the component and the phase composition of the products. A series of nanocrystalline titanium-based powders from anatase and rutile TiO_2, nitrogen-doped TiO_2, the solid solution of TiN and TiO, to phase-pure cubic TiN were prepared. This method clearly yields materials with properties being distinct from those prepared by wet-chemical methods, leading to an environmentally benign process and a less expensive product. Also, a particular pore structure (larger mesopore size) can permit high molecular weight surface species to reach the active sites existing on the catalyst surface. The up-to-bottom control over the aggregated state of nanoparticles has been demonstrated in the paper.

2. Experimental section

2.1. The synthesis of TiO_2 to TiN nanoparticles

For the synthesis of the double salt α-$(NH_4)_2TiO(SO_4)_2$, 200 g of $Ti(SO_4)_2$ was dissolved in 400 mL of distilled water, then 102 g of $(NH_4)_2SO_4$ was added into the above solution. The clear solution was placed undisturbedly. Then, a white precipitate was separated out after 3 days aging. A bulk amount precipitate was obtained (yield up to 40%) after prolonging the aging time for 15 days. When 3 M $TiOCl_2$ solution was used as titanium source instead of equimolar $Ti(SO_4)_2$, the phase of the obtained white precipitate matched with that derived from $Ti(SO_4)_2$ identically, both assigned to α-$(NH_4)_2TiO(SO_4)_2$ (JCPDS 34-0732).

For the preparation of titanium-based powders, 5 g of ammonium titanyl sulfate α-$(NH_4)_2TiO(SO_4)_2$ (ATS) was placed in a high-purity quartz boat and set in a quartz tube furnace (inner diameter 82 mm) with air-tight end gaskets. The reactor was heated in the static air, flowing Ar or NH_3 gas at a flow rate of 500 mL min^{-1} to an appropriate temperature, and

Table 1
Bulk and physicochemical properties of the samples

Sample	*T*/*t*/Atm.[a]	Phase[b]	Φ[c] (nm)	SSA[d] ($m^2\,g^{-1}$)/PV[e] ($cm^3\,g^{-1}$)	$r_0 \times 10^9$[f] ($mol\,L^{-1}\,s^{-1}$)
TiO_2-6002-air	600/2/air	A, $TiOSO_4$ (9.3%)	17.8	61.6/0.264	17.5[h]
TiO_2-6008-air	600/8/air	A	26.3	52.7/0.256	25.1
TiO_2-70005-air	700/0.5/air	A	25.6	66.4/0.273	25.0
TiO_2-7002-air	700/2/air	A	26.2	64.5/0.266	25.9
TiO_2-8002-air	800/2/air	A, R (3.0%)	39.3A	22.8/0.037	18.8
TiO_2-9002-air	900/2/air	A, R (79.4%)	81.2R	7.0/0.013	9.7
TiO_2-6002-Ar	600/2/Ar	A, $TiOSO_4$ (8.8%)	16.9	68.4/0.281	18.1[h]
TiO_2-6502-Ar	650/2/Ar	A, R (9.1%)	22.1A	64.3/0.279	28.7
TiO_2-7002-Ar	700/2/Ar	A, R (86.7%)	70.5R	11.2/0.045	15.1
TiO_2-7502-Ar	750/2/Ar	A, R (91.1%)	75.6R	10.2/0.023	13.4
TiO_2-6005-NH_3	600/5/NH_3	A	27.0	59.4/0.254	8.5
$TiO_{2-x}N_x$[g]	400/0.5/Air	A	27.0	47.9/0.218	12.6
P-25	Degussa	A, R (20%)	27.2A	50.5/0.097	25.1
TiO_2-6505-NH_3	650/5/NH_3	A, c-TiN	–	55.3/0.247	–
TiO_2-7005-NH_3	700/5/NH_3	c-TiN	–	48.7/0.224	–
TiO_2-8003-NH_3	800/5/NH_3	c-TiN	–	36.5/0.083	–

[a] *T*/*t*/Atm.: TD temperature/holding time/atmosphere.
[b] A: anatase, R: rutile.
[c] Φ: diameter of crystallites calculated by the Scherrer equation.
[d] SSA: BET specific surface area.
[e] PV: pore volume at $P/P_0 = 0.97$.
[f] r_0: initial reaction rate for MB degradation.
[g] $TiO_{2-x}N_x$ was prepared by post-calcination of the sample TiO_2-6005-NH_3 at 400 °C for 0.5 h in air.
[h] Before being used as photocatalysts, samples TiO_2-6002-air and TiO_2-6002-Ar were well washed with distilled water to remove a small amount of $TiOSO_4$ remained in the samples.

held for 2–8 h. The released SO_3 or the excessive NH_3 was absorbed by dilute ammonia solution or dilute sulfuric acid, respectively. The aims of varying atmospheres are to tune the phase as well as the component of the resulting titanium-based powders. Thus, anatase or rutile TiO_2, nitrogen-doped TiO_2, TiN_xO_{1-x}, and TiN powders were obtained upon the thermal decomposition of ATS, the detailed conditions for the preparation of each one was summarized in Table 1.

2.2. Sample characterization

The powder phase composition was identified by X-ray diffraction (XRD) equipment (Model D/max 2550V, Rigaku Co. Tokyo, Japan), using Cu Kα ($\lambda = 1.5406$ Å) radiation. The broadening of XRD peak at $2\theta = 25.4°$ (d_{101}) for anatase TiO_2, and $2\theta = 27.3°$ (d_{110}) for rutile TiO_2, was used to calculate the crystallite size according to the well-known Scherrer equation. The morphology and the crystallite size of the resultant TiO_2 were observed using a transmission electron microscopy (TEM; Model JEM-200CX, JEOL Tokyo, Japan) and field emission scanning electron microscopy (FE-SEM; Model JSM-6700F, JEOL, Tokyo, Japan). The BET specific surface area measurement was performed on a nitrogen adsorption apparatus (Model ASAP 2010, Micromeritics Instruments, Norcross, GA, USA). Diffuse reflectance spectra (DRS) were recorded on a Shimadzu UV-3101 PC instrument, using $BaSO_4$ as reference sample in the range 200–800 nm. Thermogravimetry (TG) and differential scanning calorimetry (DSC) were performed on Netzsch STA 449C at the rate of 5 °C min^{-1} in flowing air or Ar gas. Elemental analysis for carbon (C), hydrogen (H) and nitrogen (N) contents in the nitride powder was carried out on a Perkin Elmer CHN analyzer (Model 2400-II, MA, USA), and O_2 was introduced into the system for the complete combustion.

2.3. Photocatalytic degradation of MB over TiO_2 nanoparticles

The methylene blue ($C_{16}H_{18}N_3SCl{\cdot}3H_2O$) was used as supplied, and its degradation was tested as a model reaction to evaluate the photocatalytic activity of the resulting TiO_2 and nitrogen-doped TiO_2 powders. The photocatalytic experiments were carried out by adding 0.32 g of TiO_2 powder into 450 mL Pyrex photoreactor containing 400 mL of 5.35×10^{-5} M (20 mg L^{-1}) methylene blue (MB) solution. The cooling water in a quartz cylindrical jacket round the lamp was used to keep the reaction temperature constant (22 ± 2 °C). Before illumination, the suspension containing catalyst and MB was sonicated for 5 min and stored in dark for further 25 min to obtain the saturated absorption of MB. Then, the stirring suspension was illuminated by means of 300 W medium pressure Hg lamp with a filter (ZJB 340 filter glass, Shanghai Non-ferrous Glass Ltd.) to cut off the light with wavelength <340 nm to determine the photocatalytic activity under UV–vis light irradiation. The light energy distribution of the light source was reported elsewhere.[27] The pH of the solution was adjusted to 6.5 after methylene blue dissolved in distilled water. O_2 was continuously bubbled into aqueous suspension at a flow rate of 100 mL min^{-1} for 0.5 h before switching on the lamp and throughout the occurrence of the photoreactivity experiments. After UV–vis light illumination, 2 mL aliquot of reaction mixture was taken

out at regular time intervals, and was diluted to 10 mL with the distilled water. The catalyst was removed from solution by a centrifuger at 6000 rpm and the supernatant was used for the quantitative analysis of MB. The change in the concentration in each degraded solution was monitored on a Shimadzu UV-1601 spectrophotometer by measuring the absorbance of MB at 655 nm. For comparison, the photocatalytic activity of the commercial Degussa P-25 under UV–vis light irradiation was tested in the MB degradation reaction.

3. Results and discussion

3.1. TGA–DSC investigation

To optimize the temperature for the decomposition of ATS, thermalgravimetric analysis (TGA) and DSC analysis were performed on the ATS powder in flowing air or Ar gas. This TGA–DSC analysis could determine the temperature at which the ATS began to decompose. The TGA–DSC analysis results are shown in Fig. 1, and there are four peaks in the DSC curve. At approximately 472 °C, a strong endothermic peak is observed, which may come from the decomposition of ATS as shown in Eq. (1) due to a distinct weight loss occurred around the temperature. The weaker peak at 508 and 557 °C are assigned to the melting or further decomposition of solid state mixture or intermediate such as $(NH_4)_2TiO_2SO_4$. In the handbook edited by Dean,[28] one can find the decomposition temperature is 230 and 350 °C for $(NH_4)_2SO_4$ and NH_4HSO_4, respectively. Both of them are much lower than the first peak (472 °C) in DSC curve. We assume that the relatively high thermal stability of $(NH_4)_2SO_4$ and NH_4HSO_4 arises from the interaction of $(NH_4)_2SO_4$ with $TiOSO_4$ after molecular level mixing in the single-crystal ATS. From the XRD and TEM results given in the following sections, it is seen that a small amount of $TiOSO_4$ remains in the product TiO_2-6002-air, which indicates the peak at 609 °C in DSC curve is assigned to the decomposition of $TiOSO_4$. The TGA curve shows two stages, the first one accompanies a weight loss 27% and the total weight loss is up to 72.3%, which is well-consistent with 72.6% according to Eq. (3).

$$\text{Step I}: (NH_4)_2TiO(SO_4)_2(s) \rightarrow (NH_4)_2TiO_2SO_4(s) + SO_3(g) \quad -27.4\,\text{wt.\%} \tag{1}$$

$$\text{Step II}: (NH_4)_2TiO_2SO_4(s) \rightarrow TiO_2(s) + 2NH_3(g) + SO_3(g) + H_2O(g) \quad -45.2\,\text{wt.\%} \tag{2}$$

$$\text{Total reaction}: (NH_4)_2TiO(SO_4)_2(s) \rightarrow TiO_2(s) + 2NH_3(g) + 2SO_3(g) + H_2O(g) \quad -72.6\,\text{wt.\%} \tag{3}$$

The TGA–DSC analysis of ATS was also carried out in flowing air, which is very similar to that in flowing Ar gas as shown in Fig. 1. No exothermic peak corresponding to anatase to rutile transformation is detected in DSC curves for both atmospheres, which may be interpreted in view of the very slow rate of anatase to rutile transformation and the low change of the transformation free energy.[29,30]

3.2. XRD and N_2-sorption measurements

Fig. 2 shows XRD patterns of the as-prepared ATS and its calcined products at varying temperatures in air or flowing Ar gas. The names of calcined samples were abbreviated, and conditions for the preparation of each sample were listed in Table 1. TiO_2-6002-air consists of major anatase TiO_2 and a small amount (9.3 wt.%) of orthorhombic $TiOSO_4$, suggesting 600 °C is not high enough to decompose $TiOSO_4$ completely. Prolonging the calcining time or raising the calcining temperature promotes the complete decomposition of $TiOSO_4$. However, prolonging the calcining time generally formed more connected anatase nanocrystals as observed by TEM (see the Supporting Information, Figure

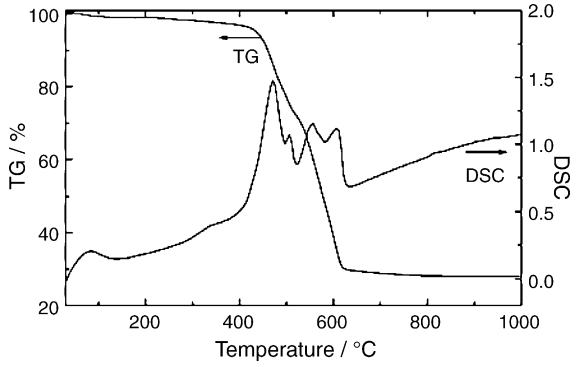

Fig. 1. TGA–DSC curves of α-$(NH_4)_2TiO(SO_4)_2$ precursor in flowing Ar gas.

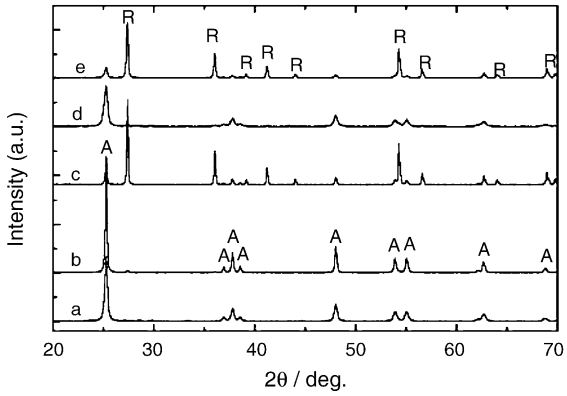

Fig. 2. XRD patterns of TiO_2 powder by the thermal decomposition of ATS. (a) TiO_2-7002-air, (b) TiO_2-8002-air, (c) TiO_2-9002-air, (d) TiO_2-6502-Ar and (e) TiO_2-7002-Ar. A and R represent anatase and rutile, respectively.

S1), and the more connected TiO_2 powder possessed a lower surface area (Table 1). Upon the decomposition of ATS in the static air, rutile occurs at 800 °C or above, which results in a drastic loss of surface area and porosity. The product TiO_2-9002-air is predominantly composed of rutile (79.4%), due to the anatase-to-rutile transformation. It is interesting that the predominant rutile TiO_2 powders could be obtained at much lower temperatures in flowing Ar gas. For instance, the product TiO_2-7002-Ar is predominantly composed of rutile (86.7%), and the temperature for the preparation of TiO_2-7002-Ar is 200 °C lower than that for the preparation of TiO_2-9002-air although the dynamically growth of rutile were observed at 700 °C. We tentatively proposed the occurring of rutile at relatively lower temperature is due to the fast removal of SO_3 gas in flowing Ar gas. Therefore, less sulfate ions were trapped or absorbed on the surface of TiO_2 nanocrystals, and sulfate ions are believed as an effective stabilizing agent of anatase TiO_2 against anatase to rutile transformation.[31]

Fig. 3 shows XRD patterns of the ATS after post-calcination in flowing NH_3 gas. The color of TiO_2-6005-NH_3 was brown-gray, which was similar to the nitrogen-doped TiO_2 ($TiO_{2-x}N_x$) photocatalyst. $TiO_{2-x}N_x$ is a recently developed photocatalyst under visible light illumination.[32] When ATS decomposed at 650 °C or above, the solid solution of TiN_xO_{1-x} and cubic TiN were formed depending on the temperatures and thus the color of the products was turned from dark-blue to golden-brown. The only phase of solid solution TiN_xO_{1-x} was detected for the sample TiN-7005-NH_3, suggesting that TiO_2 formed during the thermal decomposition was highly reactive to NH_3 molecules. Also, the temperature 700 °C is much lower than that (800 °C or above) for complete nitridation of nanosized anatase TiO_2 derived from wet-chemical route.[33] It is noticeable that the products obtained by nitridation in the range from 650 to 900 °C are solid solution of TiN_xO_{1-x} rather than TiN powder.[34] The decrease in the d values with a decrease in the nitrogen content

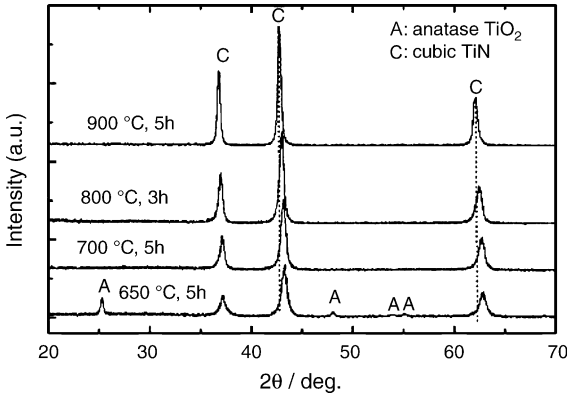

Fig. 3. XRD patterns of TiN-based powders by the thermal decomposition of ATS in flowing NH_3 gas. The powder obtained from nitridation of ATS at 650 °C for 5 h consists of a small amount of anatase TiO_2 and predominant solid solution of TiN and TiO while the one by nitridation of ATS at 900 °C for 5 h essentially consists of phase-pure cubic TiN.

Table 2
Lattice parameters and nitrogen contents of TiN_xO_{1-x} and TiN powders

Samples	Phase	Lattice constant, a (Å)	N content[b], wt.%
TiO_2-6505-NH_3	A[a], cubic	4.179	n.d.[e]
TiN-7005-NH_3	Cubic	4.189	16.18
TiN-8003-NH_3	Cubic	4.201	19.14
TiN-8005-NH_3	Cubic	4.209	19.62
TiN-9005-NH_3	Cubic	4.228	21.68
TiN-9505-NH_3	Cubic	4.239	22.22[f]
TiN[c]	Cubic	4.241	22.61
TiO[d]	Cubic	4.185	0

[a] A: anatase TiO_2.
[b] Elemental analysis for carbon (C), hydrogen (H) and nitrogen (N) contents in the nitride powder was carried out on a Perkin Elmer CHN analyzer and O_2 was introduced into the system for the complete combustion nitride powder.
[c] JCPDS 38-1420 card.
[d] JCPDS 77-2170 card.
[e] n.d. stands for not determined.
[f] The TG-DSC analysis were also carried out for this sample in air (TiN to be oxidized to TiO_2 in air), TG shows a weight increase of 28.51 wt.% and which is slightly lower than 29.06 wt.% for the stoichiometric TiN.

confirms the formation of a solid solution in TiN_xO_{1-x} powders. Table 2 gives the lattice parameters as well as nitrogen contents in the resulting titanium (oxy)nitrides.

As shown in Fig. 1, a remarkable weight loss about 72% is accompanied when ATS decomposes. Therefore, many pores are remained in the products after its decomposition. Fig. 4 shows the pore size distribution of the samples obtained from ATS after calcination at different temperatures. The pore size distribution was calculated using the BJH method. For comparison, the pore size distribution of Degussa P-25 is given, and it is a non-porous photocatalyst.[1,4] The mean pore size, pore volume, and the crystallite size of Ti-based nanocrystals are listed in Table 1. The distribution profiles of all the curves were different, but the maximum of the pore size distribution for the sample TiO_2-6002-A and TiO_2-7002-A were almost identical. Both of them show a mesoporous textural structures with an average pore diameter around 15 nm, which is larger than that of wet-chemical-derived TiO_2 (less than 4–10 nm depending on the preparative conditions).[22]

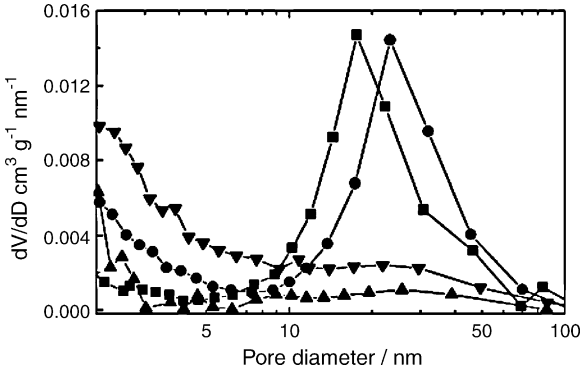

Fig. 4. Pore size distribution of TiO_2 powders. (■)TiO_2-6002-air, (●)TiO_2-7002-air, (▲)TiO_2-8002-air, and (▼) Degussa P-25.

The large mesopores may be beneficial for photocatalysis since the more accessible active sites are available for the photocatalytic process. Moreover, the larger size and better connectivity of mesopores provides more pathways for the reactants to enter and products to escape from the network. These mesoporous characteristic is crucial to photocatalytic reactions especially to degrade large-molecular pollutants. For the sample TiO_2-8002-air, the pore size distribution was similar with that of Degussa P-25. The sample TiO_2-8002-air was partially sintered and has a lower specific surface area and pore volume and those may result in its lower photocatalytic activity for the degradation of MB.

Upon the thermal decomposition of ATS, all mesopores are not created equal and thus the photocatalysts are disordered materials. As recently reviewed by Rolison,[23] the orderedly mesoporous materials derived from the surfactant-templated approach is not ideally ready to be applied to catalysis due to they potentially suffer from a plumbing problem because the periodic porosity is one-dimensional and nanoscopic, and internal blockage shuts off the catalyzed walls of that pipe from reaction. Our prepared anatase TiO_2 powders with disordered mesopores are expected as highly efficient heterogeneous catalysts.

3.3. SEM and TEM images

Fig. 5 depicts the FE-SEM images of α-$(NH_4)_2TiO(SO_4)_2$ (ATS) precursor and the TiO_2 powder derived from it. Most of the single crystal ATS particles are fibrous-like with diameters around 1.5 μm and lengths up to 10 μm. Upon the thermal decomposition of ATS, the original morphologies of ATS are preserved but in some cases the shrinkage of dimensions is also observed due to the remarkable loss of mass during the decomposition process. The resulting 2D or 3D TiO_2 nanoarchitectures are porous, and many mesopores are detected distinctively by FE-SEM. Besides more accessible active sites and easier transported pathways, 3D TiO_2 network has other advantages over the discrete nanoparticles. The larger nanoarchitectures of TiO_2 nanocrystals can be decanted from the treated solution or be rapidly and easily recovered by a less energy-consumed filtration process (common filter paper is enough to recover the photocatalyst) after each cycle. The characteristics of 3D TiO_2 network make it can be act as an ideal catalyst for heterogeneous catalysis especially photocatalysis.

The structural hierarchy of the resulting Ti-based powder is further recognized by TEM. Fig. 6 depicts TEM images of some products. It is shown that the samples consist of connected particles rather than the discrete nanoparticles. As we expected, the dimensions are up to 2 μm × 2 μm (see the Supporting Information, Figure S2). In some cases, the nanostructured architectures with a thickness of ca. 20 nm are just like the assembled monolayers of TiO_2 nanocrystals while some mesoporous spheres and fibers are also seen (see the Supporting Information, Figure S2). These monolayers of TiO_2 nanocrystals are also used to prepare particulate TiO_2 thin films on different substrates as immobilized photocatalysts. Moreover, unlike most bottom-to-up assembling, the simple and facile route will be developed to obtain Ti-based powders from TiO_2 to TiN with predetermined aggregated-states and size by effectively controlling the morphology and size of the single-crystal ATS precursor. The porous nanosheets and spheres or fibers correspond to 2D and 3D network, respectively. The anatase products TiO_2-6002-air, TiO_2-7002-air and TiO_2-6502-Ar consist of TiO_2 nanocrystals in the size of 15–20, 20–30 and 15–25 nm, respectively. Correspondingly, the specific surface areas of these samples are 61.6, 64.5 and 64.3 $m^2\,g^{-1}$. The specific surface area of TiO_2-6002-air is lower than that of TiO_2-7002-air due to the existence of $TiOSO_4$ in micrometer-size, which has little contribution to the specific surface area. It is notable that the surface area of TiO_2-7002-air and TiO_2-9002-air is relatively higher than that of titania powders derived from Wet-chemical methods after post-calcination at such high temperatures. After post-calcination at 700 °C in air, emulsion-mediated TiO_2 had a surface area of 5.9 $m^2\,g^{-1}$g.[24,35] Sibu et al.[36] reported that the specific surface area of TiO_2 powder after calcination at 700 °C was 1 $m^2\,g^{-1}$, and could be increased to as high as 52 $m^2\,g^{-1}$g in the presence 1% La_2O_3. Kominami

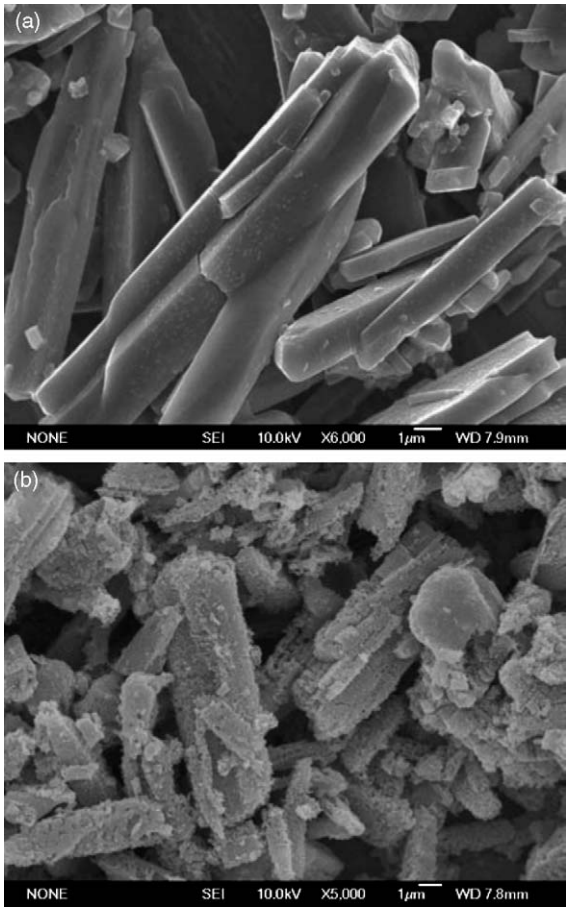

Fig. 5. SEM images of (a) as-prepared α-$(NH_4)_2TiO(SO_4)_2$ precursor and (b) TiO_2-6502-Ar.

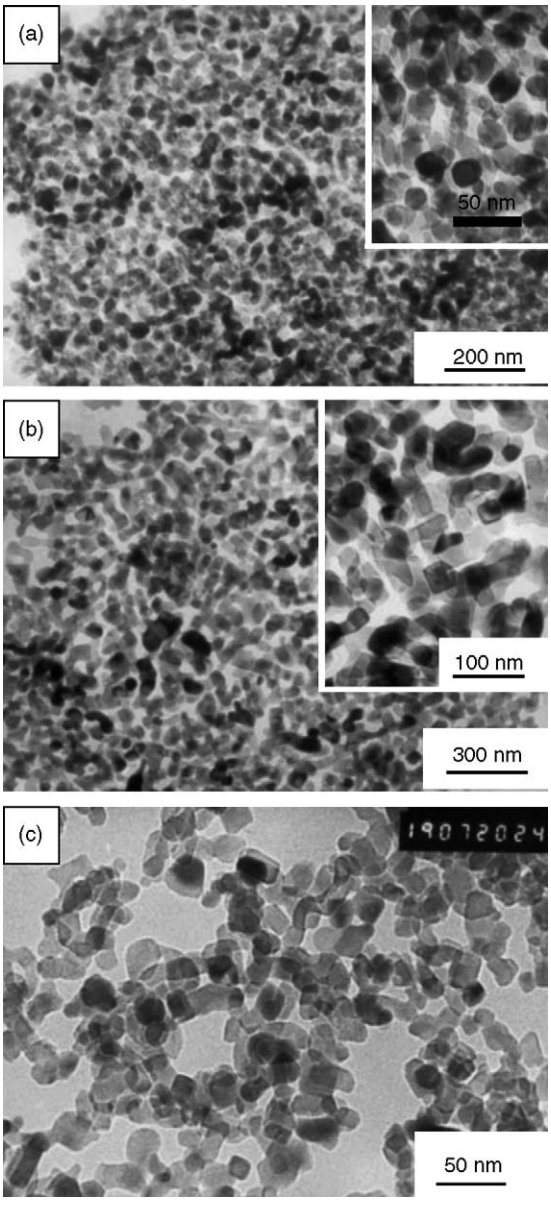

Fig. 6. TEM images of as-prepared nanocrystalline TiO_2 obtained by thermal decomposition of α-$(NH_4)_2TiO(SO_4)_2$. (a) TiO_2-6002-air, (b) TiO_2-7002-air and (c) TiO_2-6502-Ar.

et al. prepared extremely stable anatase nanoparticles by hydrothermal crystallization in organic media (HyCOM), and the samples after post-calcination at 700 °C had a specific surface area between 21 and 69 $m^2\,g^{-1}$g depending on HyCOM conditions.[37] Other methods to keep high stability of TiO_2 nanoparticles against particle growth include the formation of a metastable solid solution on the surface of oxide nanoparticles[38] or the replacement of the surface hydroxyl groups with another functional group.[39] During the thermal decomposition of ATS, neither dopants nor additives are introduced into the samples, and they still retain remarkably high surface area. The remarkably thermal stability of the TiO_2 powder derived from the thermal decomposition of ATS can be explained in view of its high porosity as well

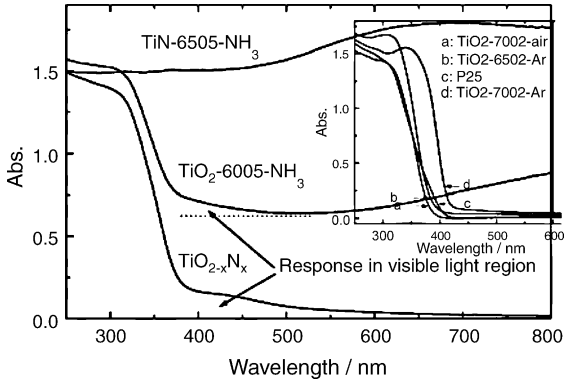

Fig. 7. UV–vis diffuse reflectance spectra (DRS) of TiO_2 and nitrogen-doped TiO_2 powders. The preparation conditions of these samples are listed in Table1, the DRS of Degussa P25 is also given in this figure for comparison.

as the large-sized mesoporous nature. It is known that the micropores and mesopores with a diameter less than 5 nm may collapse at the temperature around 400–600 °C.[20]

3.4. UV–vis spectra

Fig. 7 depicts the diffuse reflectance spectra of some samples. The spectra of TiO_2-7002-air and TiO_2-6502-Ar correspond to anatase TiO_2, and the spectrum of Degussa P-25 is very similar to that of anatase but with an onset of absorption band gap at 410 nm corresponds to rutile TiO_2. The spectrum of TiO_2-7002-Ar is very similar to that of rutile TiO_2 since rutile is the predominant phase in this product. Both the spectra of TiO_2-6502-Ar and TiO_2-7002-Ar consist of a weak tail in the visible light region, which may suggest that the intermolecular NH_3 arising from decomposition of ATS acts as nitridation agent to dope TiO_2 nanocrystals. However, the response in the visible light region is very weak compared to that of recently intensively investigated $TiO_{2-x}N_x$ photocatalyst.[32] The spectrum of the TiO_2-6005-NH_3 shows a noticeable response in visible light region (extend to 500 nm), similar to excessively nitrided TiO_2 nanoparticles as reported by Irie et al.[32] Meanwhile, an increase in absorption extended to 800 nm (the absorbance in the region 500–800 nm is much higher than zero) is observed, which may be assigned to the formation of Ti^{3+} and which is believed with a band gap between 0.75 and 1.18 eV.[40] Besides the contribution of Ti^{3+} to the visible light response, we suggest the metallic nature of TiN_xO_{1-x} and TiN also significantly affect their UV–vis spectra, which is analogous to the Pt/TiO_2 system. The metallic Pt clusters change significantly the UV–vis spectra even at very low content of 0.1 wt% (0.02% in volume) to the TiO_2 powder.[41] Driessen and Grassian interpreted the UV–vis spectra of Pt/TiO_2 system according to Maxwell–Garnett theory, and found the experimental absorption of the Pt/TiO_2 system in the visible light region was much stronger than that theoretically predicted.[41] So, for the excessively nitrided TiO_2, the presence of metallic TiN_xO_{1-x} and TiN may also contribute to a remarkable absorption of nitrogen-doped TiO_2 at much

longer wavelengths compared to pure TiO_2. This enhanced absorption in the visible light can be remarkably reduced by post-calcination of the sample at 400 °C for 0.5 h in air, and then the post-calcined sample shows the same spectrum as those recently reported.[32] Upon the thermal decomposition of ATS in flowing NH_3 gas at the temperatures ranging from 650 to 900 °C, a much stronger absorption in the visible light region was observed in the samples. For sample TiO_2-6502-Ar, the absorbance in the visible region is stronger than that in the UV light region because the cubic TiN_xO_{1-x} solid solution is the predominant phase in the sample. The titanium oxynitride (TiN_xO_{1-x} solid solution) possesses some special application such as electrically switchable window[42] due to its enhanced absorbance ability in the visible light region.

3.5. Photocatalytic activity for the degradation of MB

The photocatalytic activity has been tested in the photodegradation of aqueous solutions of MB and evaluated by comparison with Degussa P-25, which consists of 80% anatase and 20% rutile and has a specific surface area of 50 $m^2\,g^{-1}$g. As shown in Table 1, the photocatalytic activity of some samples (i.e., TiO_2-6502-Ar) is higher than that of Degussa P-25. The latter is believed a commercial photocatalyst with the highest photocatalytic activity due to the synergetic contribution by the mixing of anatase and rutile[43] and the suppressing of the recombination of photogenerated electron–hole pairs by doping small amount of Fe(III) ions.[4] The higher photocatalytic activity of TiO_2-6502-Ar can be interpreted in the view of the high crystallinity and large mesopores. The size-dependent photoredox power was reported in 1986,[44] however, with respect to TiO_2 photocatalysts, the effect of the crystallite size on the photocatalytic activity is contradictious due to other parameters such as crystalline phase, the ratio of the different phases, the substrates to be degraded, and crystallinity.[4,7,21,22] The crystallite size of ca. 15 nm in TiO_2-6502-Ar is larger than quantum-size of most semiconductors (around 10 nm or less), its higher photocatalytic activity is most likely arising form the more available photo-generated electrons rather than the enlarged redox potential. As pointed out by Grätzel et al., the diffusion of conduction band electrons from the interior to the surface as well as their subsequent relaxation into the trapping surface states is a very rapid process for TiO_2 nanocrystals in the size of 12 nm compared to larger particles.[45]

Fig. 8 compares the degradation rates over different photocatalysts, and the significantly enhanced photocatalytic activity is observed for the TiO_2 nanocrystals in the anatase phase. The size-dependent photocatalytic activity of anatase TiO_2 nanocrystals were observed, for example, the sample TiO_2-8002-air shows much lower photocatalytic activity compared to that of TiO_2-7002-air or TiO_2-6502-Ar. The mean degradation rate (irradiating time 0.5 h) for the sample TiO_2-6502-Ar is as high as 28.7×10^{-9} mol L^{-1} s^{-1} whereas TiO_2-8002-air shows a much lower degradation rate of 18.8×10^{-9} mol L^{-1} s^{-1}. The degradation rate over

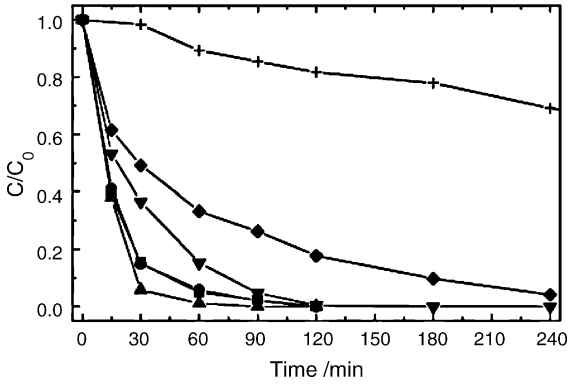

Fig. 8. The concentration changes of methylene blue (5.35×10^{-5} M) over TiO_2 photocatalysts under UV–vis light irradiation at pH 6.5. (+) Without catalyst, (♦) TiO_2-7002-Ar, (▼) TiO_2-8002-air, (■) Degussa P-25, (●) TiO_2-7002-air, and (▲) TiO_2-6502-Ar. The physicochemical properties of photocatalysts are listed in Table 1.

the sample TiO_2-6502-Ar is higher than that of Degussa P-25, which also falls in the same order as that reported.[46] Many works focused on the effects of crystallinity, particle size, and preparative methods on the photocatalytic activity have been done.[4,7,21,22,37] In the present work, we stress that besides these crucial parameters, the large size of mesopores in the nanostructured TiO_2 may also be very beneficial to photocatalytic degradation for organic pollutants especially pollutants with relatively large molecular size. The large and connected mesopores not only allows more active sites available for heterogeneous catalysis but also provides much more pathways for mass transferring during the photocatalytic process. It is notable that the samples in the predominant rutile phase also removes MB from the solution at relative high rate after taking into consideration their low specific surface area. The samples in the predominant rutile phase were mesoporous (see the Supporting Information, Figure 2) but their crystallite size is much larger than that of anatase TiO_2 samples. Many works concluded rutile TiO_2 is inactive to be applied as photocatalyst due to its higher hole–electron recombination rate[47] and its more dehydroxylated surface,[7] and we previously demonstrated that the calcined rutile (in other words, rutile with a larger crystallite size) showed a significantly reduced photocatalytic activity for the photocatalytic degradation of phenol.[48] As shown in Fig. 8, the photocatalytic activity of TiO_2-6005-NH_3 and $TiO_{2-x}N_x$ is lower than that of the prepared TiO_2 photocatalysts and Degussa P-25 under UV–vis light irradiation. However, the nitrogen-doped TiO_2 nanocrystals are photoactive under visible light irradiation.[32] The initial rate of TiO_2-6005-NH_3 and $TiO_{2-x}N_x$ is 8.5×10^{-9} and 12.6×10^{-9} mol L^{-1} s^{-1}, respectively, both are much lower than that of Degussa P-25 (25.1×10^{-9} mol L^{-1} s^{-1}).

The different morphology of the particles give rise to suspensions with different extinction (absorption and scattering) characteristics.[49] The 250–800 nm spectrum of the diluted suspension was measured in 1 cm path length cells in this paper. Fig. 9 shows the extinction (absorption and scattering)

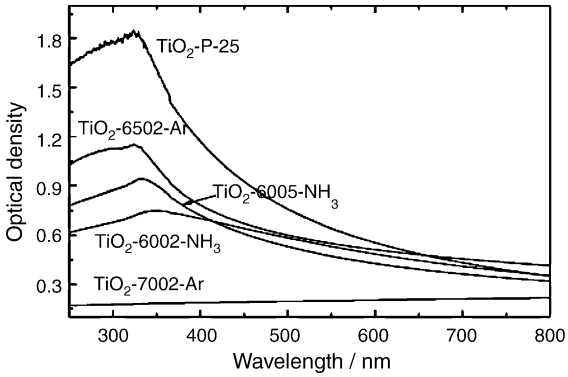

Fig. 9. The extinction (absorption and scattering) spectra of 1 mM diluted suspensions of the selected TiO_2 samples.

spectra of TiO_2 suspensions of the selected samples. The suspension of P-25 absorbs and scatters more light in the UV–vis region, due to the finer size of aggregates in Degussa P-25 (about 700 nm[49]), the other suspensions absorbs and scatters less light due to the larger size of aggregates as shown in Fig. 5b. The sample TiO_2-7002-Ar may be somewhat sintered and the extinction spectrum of its suspension lose the absorption characteristics of colloidal TiO_2, which is similar to that of rutile TiO_2 suspension recently reported by Egerton and Tooley.[50] This increased extinction causes the UV flux incident on the slurry to be absorbed within a shorter path length, i.e., is absorbed by fewer crystals.[50] So, P-25 TiO_2 photocatalyst in this photoreactor has lower photocatalytic activity but actually comparable or higher quantum efficiency than TiO_2-6502-Ar does after taking into consideration of its absorption and scattering characteristics. A careful work to differ the individual contribution of absorption from extinction is needed and thus the quantum efficiency will be concluded.

In fact, both N-doped samples absorb not only the strongest emission peaked at 365 nm as same as undoped anatase TiO_2 but also the light with wavelength peaked at 404 and 436 nm from the medium pressure Hg lamp. The phenomenon that N-doped TiO_2 absorbs more light but possesses less photocatalytic activity may be explained according to the following aspects. The works on metal ions doped TiO_2 were intensively investigated in the last decade,[51–53] are very helpful to understand the lower photocatalytic activity of nitrogen-doped TiO_2. According to Hoffmann et al.,[52] the presence of energy levels below the conduction band edge and above the valence band edge influences the photoreactivity of TiO_2 since the metal ions act as electron (or hole) traps, altering the electron–hole pair recombination rate. The dopants are also isolated far from the surface with a low chance of transferring trapped charge carriers to the interface and therefore the metal ions act more likely as recombination centers of the photo generated e^-/h^+ pairs than trap sites.[53] In general, the nitrogen-doped TiO_2 shows a lower reactivity under UV–vis irradiation than undoped anatase TiO_2 does. Irie et al. has explained the lower activity of nitrogen-doped TiO_2, they demonstrated that the isolate lower band gap also existed in the nitrogen-doped TiO_2 and the isolate band also acts as the recombination center of the photo-generated electron–hole pair.[32] Therefore, less active species for redox reactions are available in the nitrogen-doped TiO_2. Besides this consideration, the less light harvesting also may be responsible for the lower activity of nitrogen-doped TiO_2. As shown in Fig. 7, the nitrogen-doped TiO_2 (TiO_2-6005-NH_3) absorbs some light with wavelength up to 800 nm, due to the formation of Ti^{3+}. However, the Ti^{3+} itself not only does not possess the photocatalytic activity but also acts as an absorption centre in the UV–vis region. Therefore, much less light can arrive at the photocatalyst far from the light source, which results in a much darker zone formed in the suspension containing the $TiO_{2-x}N_x$ photocatalyst. After post-calcination of the excessively nitrided TiO_2 in air at 400 °C for 0.5 h, the photocatalyst ($TiO_{2-x}N_x$ listed in Table 1) does not adsorb the light with wavelength larger than 600 nm. The $TiO_{2-x}N_x$ photocatalyst promises a wide range of applications as the solar energy material because it absorbs a lot of photons under the sunlight or the indoor lighting.

4. Conclusions

In summary, the single crystal of the double salt ATS was formed via room temperature aging by mixing of $TiCl_4$ or $TiOSO_4$ with $(NH_4)_2SO_4$ solution. After subsequent heating (600 °C and above) precursor ATS was decomposed, and the released gas could be recycled. Therefore, this is an environmentally benign route for the preparation of Ti-based powers from oxides to nitrides. The dimensions of the network of 2-D and 3-D nanocrystalline Ti-based powders (anatase/rutile TiO_2, nitrogen-doped TiO_2, $TiO_{1-x}N_x$, and TiN) were up to several micrometers. Such high-temperature processing is ideal for producing fully crystallized TiO_2 with higher thermal stability than that derived from low-temperature wet-chemical route. Moreover, the anatase TiO_2 powders derived from the thermal decomposition of ATS, have mesopores of larger pore size as well as more accessible surface/interface areas, allowing them act as a highly efficient photocatalyst in particular for the degradation of large dyes molecules. For instance, in photocatalytic degradation of MB, the network consisting of mesopores with diameters around 15 nm and anatase TiO_2 nanocrystals in the size of 20–30 nm shows a higher photocatalytic activity compared with Degussa P-25 photocatalyst.

Supporting Information

TEM images of the samples TiO_2-6008-air, TiO_2-7002-Ar, TiN-7005-NH_3, and TiN-8005-NH_3 are available free of charge on request to the corresponding author.

Acknowledgment

This work is supported by the National Natural Science Foundation of China (No. 50372079) and Shanghai Nanotechnology Promotion Center (0352nm093). Q. Zhang thanks Prof. Meiling Ruan and Mr. Wei Shi for the TEM and HRTEM analysis.

References

1. Hoffmann, M. R., Martin, S. T., Choi, W. and Bahnemann, D., Environmental applications of semiconductor photocatalysis. *Chem. Rev.*, 1995, **95**, 69–96.
2. Bach, U., Lupo, D., Comte, P., Moser, J. E., Weissörtel, F., Salbeck, J. *et al.*, Solid-state dye-sensitized mesoporous TiO_2 solar cells with high photon-to-electron conversion efficiencies. *Nature*, 1998, **395**, 583–585.
3. Pfaff, G. and Reynders, P., Angle-dependent optical effects deriving from submicron structures of films and pigments. *Chem. Rev.*, 1999, **99**, 1963–1982.
4. Zhang, Z. B., Wang, C.-C., Zakaria, R. and Ying, J. Y., Role of particle size in nanocrystalline TiO_2-based photocatalysts. *J. Phys. Chem. B*, 1998, **102**, 10871–10878.
5. Grätzel, M. and Howe, R., Electron paramagnetic resonance studies of doped titanium dioxide colloids. *J. Phys. Chem.*, 1990, **94**, 2566–2572.
6. Ding, Z., Lu, G. Q. and Greenfield, P. F., Role of the crystallite phase of TiO_2 in heterogeneous photocatalysis for phenol oxidation in water. *J. Phys. Chem. B*, 2000, **104**, 4815–4820.
7. Sclafani, A., Palmisano, L. and Schiavello, M., Influence of the preparation methods of titanium dioxide on the photocatalytic degradation of phenol in aqueous dispersion. *J. Phys. Chem.*, 1990, **94**, 829–832.
8. Andersson, M., Osterlund, L., Ljungstrom, S. and Palmqvist, A., Preparation of nanosize anatase and rutile TiO_2 by hydrothermal treatment of microemulsions and their activity for photocatalytic wet oxidation of phenol. *J. Phys. Chem. B*, 2002, **106**, 10674–10679.
9. Ito, S., Yoshita, S. and Watanabe, T., Preparation of colloidal anatase TiO_2 secondary submicroparticles by hydrothermal sol-gel method. *Chem. Lett.*, 2000, 70–71.
10. Wang, C.-C. and Ying, J. Y., Sol-gel synthesis and hydrothermal processing of anatase and rutile titania nanocrystals. *Chem. Mater.*, 1999, **11**, 3113–3120.
11. Morinaga, K., Torikai, T., Nakagawa, K. and Fujino, S., Fabrication of fine α-alumina powders by thermal decomposition of ammonium aluminum carbonate hydroxide (AACH). *Acta Mater.*, 2000, **48**, 4735–4741.
12. Uekawa, N., Kajiwara, J., Mochizuki, N., Kakegawa, K. and Sasaki, Y., Synthesis of ZnO nanoparticles by decomposition of zinc peroxide. *Chem. Lett.*, 2001, **30**, 606–607.
13. Xia, B., Lenggoro, I. W. and Okuyama, K., Novel route to nanoparticle synthesis by salt-assisted aerosol decomposition. *Adv. Mater.*, 2001, **13**, 1579–1582.
14. Parala, H., Devi, A., Bhakta, R. and Fischer, R. A., Synthesis of nanoscale TiO_2 particles by a nonhydrolytic approach. *J. Mater. Chem.*, 2002, **12**, 1625–1627.
15. Docters, T., Chovelon, J. M., Hermann, J. M. and Deloume, J. P., Syntheses of TiO_2 photocatalysts by the molten salts method application to the photocatalytic degradation of prosulfuron. *Appl. Catal. B*, 2004, **50**, 219–226.
16. Nozik, A. J. and Memming, R., Physical chemistry of semiconductor–liquid interfaces. *J. Phys. Chem.*, 1996, **100**, 13061–13078.
17. Pauly, T. R., Liu, Y., Pinnavaia, T. J., Billinge, S. J. L. and Rieker, T. P., Textural mesoporosity and the catalytic activity of mesoporous molecular sieves with wormhole framework structures. *J. Am. Chem. Soc.*, 1999, **121**, 8835–8842.
18. Zhang, L. Z. and Yu, J. C., A sonochemical approach to hierarchical porous titania spheres with enhanced photocatalytic activity. *Chem. Commun.*, 2003, 2078–2079.
19. Dag, Ö., Soten, I., Çelik, Ö., Polarz, S. and Ozin, G. A., Solventless acid-free synthesis of mesostructured titania: nanovessels for metal complexes and metal nanoclusters. *Adv. Funct. Mater.*, 2003, **13**, 30–36.
20. Li, D. L., Zhou, H. S. and Honma, I., Design and synthesis of self-ordered mesoporous nanocomposite through controlled in situ crystallization. *Nat. Mater.*, 2004, **3**, 66–72.
21. Ohtani, B., Ogawa, Y. and Nishimoto, S., Photocatalytic activity of amorphous-anatase mixture of titanium(IV) oxide particles suspended in aqueous solutions. *J. Phys. Chem. B*, 1997, **101**, 3746–3752.
22. Addamo, M., Augugliaro, V., Di Paola, A., García-López, E., Loddo, V., Marcì, G. *et al.*, Preparation, characterization, and photoactivity of polycrystalline nanostructured TiO_2 catalysts. *J. Phys. Chem. B.*, 2004, **108**, 3303–3310.
23. Rolison, D. R., Catalytic nanoarchitectures-the importance of nothing and the unimportance of periodicity. *Science*, 2003, **299**, 1698–1701.
24. Sato, S., Oimatsu, S., Takahashi, R., Sodesawa, T. and Nozaki, F., Pore size regulation of TiO_2 by use of a complex of titanium tetraisopropoxide and stearic acid. *Chem. Commun.*, 1997, 2219–2220.
25. Schattlka, J. H., Shchukin, D. G., Jia, J. G., Antonietti, M. and Caruso, R. A., Photocatalytic activities of porous titania and titania/zirconia structures formed by using a polymer gel templates technique. *Chem. Mater.*, 2002, **14**, 5103–5108.
26. Zhang, Q. H. and Gao, L., Preparation of nanocrystalline titanium oxide by decomposition of molecular precursor α-$(NH_4)_2TiO(SO_4)_2$. *Chem. Lett.*, 2003, **32**, 460–461.
27. Davydov, L., Reddy, E. P., France, P. and Smirniotis, P. G., Transition-metal-substituted titania-loaded MCM-41 as photocatalysts for the degradation of aqueous organics in visible light. *J. Catal.*, 2001, **203**, 157–167.
28. Dean, J. A., ed., *Lange's Handbook of Chemistry*. 13th ed. McGraw-Hill Book Company, New York, 1985, pIV-16.
29. Zhang, H. and Banfield, J. F., Understanding polymorphic phase transformation behavior during growth of nanocrystalline aggregates: insights from TiO_2. *J. Phys. Chem. B*, 2000, **104**, 3481–3487.
30. Kikkawa, H., O'Regan, B. and Anderson, M. A., The photoelectrochemical properties of Nb-doped TiO_2 semiconducting ceramic membrane. *J. Electroanal. Chem.*, 1991, **309**, 91–101.
31. Zhang, Q. H., Gao, L. and Guo, J. K., Effect of hydrolysis conditions on morphology and crystallization of nanosized TiO_2 powder. *J. Eur. Ceram. Soc.*, 2000, **20**, 2153–2158.
32. Irie, H., Watanabe, Y. and Hashimoto, K., Nitrogen-concentration dependence on photocatalytic activity of $TiO_{2-x}N_x$ powders. *J. Phys. Chem. B*, 2003, **107**, 5483–5486.
33. Li, J. G., Gao, L., Sun, J., Zhang, Q. H., Guo, J. K. and Yan, D. S., Synthesis of nanocrystalline titanium nitride powders by direct nitridation of titanium oxide. *J. Am. Ceram. Soc.*, 2001, **84**, 3045–3047.
34. Djaoued, Y., Taj, R., Brüning, R., Badilescu, S., Ashrit, P. V., Bader, G. *et al.*, Study of the phase transition and the thermal nitridation of nanocrystalline sol–gel titania films. *J. Non-Cryst. Solids*, 2002, **297**, 55–66.
35. Kim, E. J. and Hahn, S.-H., Microstructural changes of microemulsion-mediated TiO_2 particles during calcination. *Mater. Lett.*, 2001, **49**, 244–249.
36. Sibu, C. P., Kumar, S. R., Mukundan, P. and Warrier, K. G. K., Structural modifications and associated properties of lanthanum oxide doped sol-gel nanosized titanium oxide. *Chem. Mater.*, 2002, **14**, 2876–2881.
37. Hirakawa, T., Kominami, H., Ohtani, B. and Nosaka, Y., Mechanism of photocatalytic production of active oxygens on highly crystalline TiO_2 particles by means of chemiluminescent probing and ESR spectroscopy. *J. Phys. Chem. B*, 2001, **105**, 6993–6999.

38. Leite, E. R., Maciel, A. P., Weber, I. T., Lisboa-Filho, P. N., Longo, E., Paiva-Santos, C. O. *et al.*, Development of metal oxide nanoparticles with high stability against particle growth using a metastable solid solution. *Adv. Mater.*, 2002, **14**, 905–908.
39. Wu, N.-L., Wang, S.-Y. and Rusakova, I. A., Inhibition of crystallite growth in the sol-gel synthesis of nanocrystalline metal oxides. *Science*, 1999, **285**, 1375–1377.
40. Miyauchi, M., Takashio, M. and Tobimatsu, H., Photocatalytic activity of $SrTiO_3$ codoped with nitrogen and lanthanum under visible light illumination. *Langmuir*, 2004, **20**, 232–236, and references therein.
41. Driessen, M. D. and Grasian, V. H., Photooxidation of trichloroethylene on Pt/TiO_2. *J. Phys. Chem. B*, 1998, **102**, 1418–1423.
42. Saito, Y., Hirata, M., Tada, H. and Hyodo, M., Electrically switchable window using a suspension of TiO_xN_y particles. *Appl. Phys. Lett.*, 1993, **63**, 1319–1321.
43. Bickley, R. I., Gonzalez-Carreno, T., Lees, J. S., Palmisano, L. and Tilley, R. J. D., A structural investigation of titanium dioxide photocatalysts. *J. Solid State Chem.*, 1991, **92**, 178–190.
44. Nedeljković, J. M., Nenadović, M. T., Mićić, O. I. and Nozik, A. J., Enhanced photoredox chemistry in quantized semiconductor colloids. *J. Phys. Chem.*, 1986, **90**, 12–13.
45. Rothenberger, G., Moser, J., Grätzel, M., Serpone, N. and Sharma, D. K., Charge carrier trapping and recombination dynamics in small semiconductor particles. *J. Am. Chem. Soc.*, 1985, **107**, 8054–8059.
46. Lakshmi, S., Renganathan, R. and Fujita, S., Study on TiO_2-mediated photocatalytic degradation of methylene blue. *J. Photochem. Photobiol. A*, 1995, **88**, 163–167.
47. Okamoto, K., Yamamoto, Y., Tanaka, H., Tanaka, M. and Itaya, A., Heterogeneous photocatalytic decomposition of phenol over TiO_2 powder. *Bull. Chem. Soc. Jpn.*, 1985, **58**, 2015–2022.
48. Gao, L. and Zhang, Q. H., Effects of amorphous contents and particle size on the photocatalytic properties of TiO_2 nanoparticles. *Scripta Mater.*, 2001, **44**, 1195–1198.
49. Cabrera, M. I., Alfano, O. M. and Cassano, A. E., Absorption and scattering coefficients of titanium dioxide particulate suspensions in water. *J. Phys. Chem.*, 1996, **100**, 20043–20050.
50. Egerton, T. A. and Tooley, I. R., Effect of changes in TiO_2 dispersion on its measured photocatalytic activity. *J. Phys. Chem. B*, 2004, **108**, 5066–5072.
51. Anpo, M. and Takeuchi, M., The design and development of highly reactive titanium oxide photocatalysts operating under visible light irradiation. *J. Catal.*, 2003, **216**, 505–516.
52. Choi, W., Termin, A. and Hoffmann, M. R., The role of metal ion dopants in quantum-sized TiO_2: correlation between photoreactivity and charge carrier recombination dynamics. *J. Phys. Chem.*, 1994, **98**, 13669–13679.
53. Paola, A. D., Marci, G., Palmisano, L., Schiavello, M., Uosaki, K., Ikeda, S. *et al.*, Preparation of polycrystalline TiO_2 photocatalysts impregnated with various transition metal ions: characterization and photocatalytic activity for the degradation of 4-nitrophenol. *J. Phys. Chem. B*, 2002, **106**, 637–645.